OPEN ACCESS
Journal of Multidisciplinary Applied Natural Science Vol. 6 No. 1 (2026) https://doi.org/10.47352/jmans.2774-3047.314
Check for updates
Research Article

S/CuO/nGO Material as A Potential Antibacterial under Visible Light Irradiation

Rudy T. M. Situmeang*, Sumardi Sumardi, Syangap Diningrat Sitompul, Aniska Legia, Tri Umiana Soleha, Ni Luh Gede Ratna Juliasih, and Jarnuzi Ganlazuardi*

Received : November 12, 2024	Revised : August 20, 2025	Accepted : October 10, 2025	Online : October 25, 2025

Abstract
The search for environmentally friendly antibacterial materials with excellent performance that does not make bacteria resistant is still a challenge. In this research, S/CuO/GO nanomaterials were prepared by the sol-gel method using pectin as an emulsifying agent. After freeze-drying and calcining processes, the prepared nanomaterials were characterized using XRD, UV-vis diffuse reflectance, FTIR, SEM-EDX-mapping, and TEM. The Gram-positive and Gram-negative antibacterial tests were done using the MIC and Kirby-Bauer disc diffusion methods. The characterization data showed that the antibacterial material has met the nano-size of 16 nm, and its antibacterial tests using the MIC method gave promising results. Furthermore, the best MIC test results for *Escherichia coli* and *Bacillus sp.* bacteria were obtained at a concentration of 0.01000 and 0.00125 mg/mL, respectively. In addition, the Kirby-Bauer disc diffusion antibacterial testing for *E. coli* and *B. subtilis* produced a clear zone of 12 and 18 mm with an exposure time of 15 and 30 min, respectively. These results proved that S/CuO/nGO is potent for antibacterial application.

Keywords: antibacterial agent, photocatalyst, nanomaterial, visible light

1. INTRODUCTION

The search for antimicrobial active materials is still ongoing recently. The demand is increased due to excessive use of antibiotics that can cause the resistant strains of microbial, therefore, the drug material does not able to kill the microbes completely [1][2]. As a result, microbes that are able to survive will be resistant to the previous antimicrobial drug dose. So that, alternative antimicrobial materials that cannot cause immune effects need to be sought.

Recent advances in inorganic-organic nanocomposites have demonstrated promising antibacterial performance under visible light irradiation. Several examples of materials that provide very promising results as Gram-positive and Gram-negative antibacterials are explained as follows. Functionalized cellulose is really emerging an excellent antibacterial activity nanomaterial [3]. Nano graphene oxide (nGO) itself, turns out to be able to function widely as an antibacterial agent [4]. Combining nGO with double antibiotic paste (DAP) could increase its activity to kill microbial pathogen ameliorate significantly [5].

Furthermore, metal oxides, copper(II) oxide nanoparticle (CuO NP) can be used as an efficient both antibacterial agent and nano-fertilizer [6][7]. The CuO/Cu_2O NP is potential to kill the foodborne pathogen after 5 h incubation at room temperature [8]. In addition, another research group is also showed that monodispersed Cu_2O NP has an excellent potential antibacterial and therapeutic applications with the minimum inhibition concentration (MIC) result of 0.0625 mg/mL [9]. The use of composites such as CuO and ZnO metal oxides impregnated on Ag, and $ZnO/Ag@SiO_2$, each proved to provide excellent efficiency as antibacterials, 91–99% and MIC test of 0.25 mg/mL [10][11]. Zeolitic-imidazolate-frameworks (ZIFs) is able to significantly reduce the biomass of pre-biofilm formation of phatogenic bacteria and has low cytotoxicity [12]. Then, metal organic frameworks (MOFs) in combination with other materials, can act as a platform to kill bacteria effectively through the synergistic effect of multiple types of mechanisms [13]. Changing the size of the metal or metal oxide to nanosclae and modifying the metal or metal oxide in the porous structure can provide a more promising antibacterial function.

In addition to find nanomaterials that have good antibacterial activity, material preparation that considers environmental impacts is also a focus for

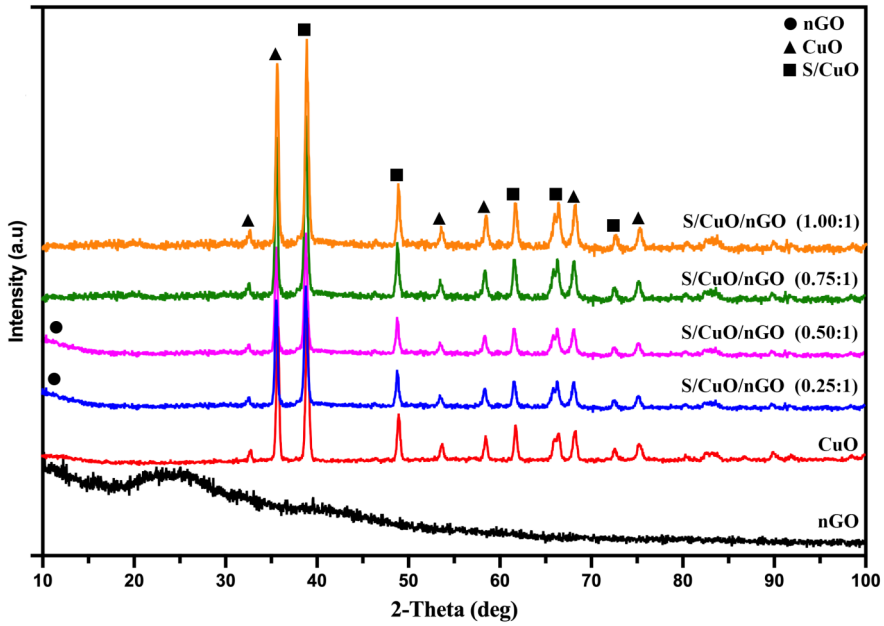

Figure 1. Difractogram of S/CuO/nGO in different ratio.

current research groups. Some examples of preparations that use environmentally friendly methods are the synthesis of Pt NPs using plant extracts such as epigallocatechin gallate (EGCG) [14][15]. Silver- or nickel and copper oxides–PVA/ starch/chitosan, and antibacterial materials dispersed in medicinal plant nanofibers [16]-[18]. This green preparation method is able to provide good material activity such as skin protectors, and food packaging. Apart from that, the material concentration required is very small, only 80 nM.

Furthermore, more complex modifications have also been carried out on several nanocomposites by combining active phases such as Cu_2O with ZnO attached to GOs [19] and CuO/Ag_2O–GO system [20] provides extraordinary antibacterial activity. Analogously, the TiO_2–CuO embedded in GO has good MIC values of 2.5 and 5.0 mg/mL for *E. coli* dan *S. aureus*, respectively [21]. Combining two or more metal oxides as active phases to porous structures, such as TiO_2 or GO, aims to promote electrons from HOMO to LUMO levels with lower energy so that the spectrum range that acts as an antibacterial in visible light is more pronounced. In addition to, the choice of GO as a metal oxide or composite active phase support is based on its characteristics in preventing agglomeration and facilitating control of the release of metal ions thereby improving the performance of the composite material. Furthermore, GO able to produce reactive oxygen species (ROS) and interact with bacterial membrane [22]. Another consideration on choosing sulfur as one of the active components because sulfur has been used since ancient times as an antiseptic. Recent studies suggest that sulfur has better antibacterial capabilities when combined with chitosan [23], and if it combined with TiO_2 providing 75% activity to prevent bacterial growth [24]. Based on the description of the related literatures above, the combination of sulfur and CuO which are distributed on GO, will be challenging for its application as antibacterial on Gram-positive and Gram-negative bacteria.

Therefore, this research concerns the nanomaterials synthesis of S/CuO embedded on nGO as composites. The preparation had been done using the green-chemistry method and the characterization is thoroughly examined using both morphological and spectroscopic techniques. These analyses providing the valuable insights into how the antibacterial materials perform. The antibacterial properties assessment of the synthesized composites, the Kirby-Baurer disk diffusion assays together with MIC, using *E. coli* as Gram-negative and *Bacillus sp* as Gram-positive representing model bacteria. By comparing the antibacterial activity of CuO, S/CuO, and S/CuO/ nGO, the aims of this research are to highlight the potential of S/CuO/nGO composites and to expand

the availability of nanomaterials in combating bacteria.

2. MATERIALS AND METHODS

2.1. Materials and Reagents

Equipment needed for this research includes stirring rods, spin bar, ice bath, desiccator, sonicator, pH meter, incubator, petri dish, laminar air flow, Bunsen, stopwatch, microscope, analytical balance, centrifuge and tubes, *aluminum foil*, *hot plate stirrer*, test tubes and its racks, oven, furnace, desiccator, visible lamp, catalytic reactor, thermometer, glass funnels, Erlenmeyer and volumetric flasks, beaker, mortar and pestle, vials, and spray bottle. The materials prepared for use in this research are corncob powder, $NaNO_3$ (99.9%), $FeCl_3 \cdot 6H_2O$ (³ 98%), NaOH 1 M, $Cu(NO_3)_2 \cdot 3H_2O$ (99.5%), HCl 1 M, HCl 5%, aquadest, natural graphite of synthesis result, H_2SO_4 (95%), H_2O_2 (30%), $KMnO_4$ (99.0%), $BaCl_2 \cdot 2H_2O$ (99%), pectin (food grade), alcohol, nutrient agar, endo agar, nutrient broth, lactose broth, brilliant green lactose broth, and cotton.

2.2. Synthesis of Nano-CuO

A total of 12 g of pectin was dissolved in 400 mL of distilled water then stirred until homogeneous for approximately 3 h. On the other hand, 400 mL of 0.157 M Cu $(NO_3)_2$ is prepared and put into 2 infusion bottles of the same volume and the speed is adjusted so that it runs out simultaneously when added to the pectin solution, accompanied by the addition of ammonia solution up to pH 11. The sample is stirred and heated at a temperature below 80 °C until a gel forms, then put in the refrigerator until frozen. Furthermore, the frozen gel was freeze-dried for 55 h and calcined for 1 h at 700°C. The CuO formed is then analyzed to determine the crystalline phase formed [25][26].

2.3. Synthesis of Nano-nGO

GO nanosheets were prepared in two steps, namely oxidation of natural graphite powder via the modified Hummers method and ultrasonication. In the first step, 2.5 g of $NaNO_3$ and 5 g of natural graphite were dissolved in a glass beaker using 120 mL H_2SO_4 (95%), and stirred for 10 min while being placed in an ice bath until the temperature was below 5 °C. A 15 g of $KMnO_4$ was added slowly while stirring and cooling so that the mixture temperature was maintained below 5 °C for 3 h. The mixture was then removed from the ice bath and then heated at 98 °C for 15 min while adding distilled water to 400 mL. A total of 15 mL of H_2O_2 solution was added slowly. The resulting GO suspension was then centrifuged with 5% HCl solution which was then tested using $BaCl_2$, then

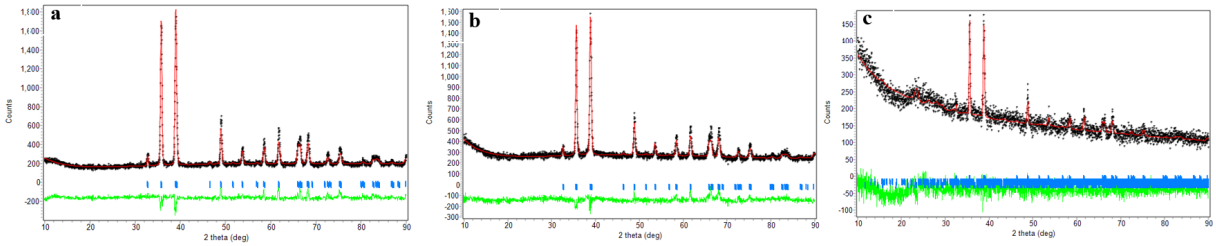

Figure 2. Rietica method using to identify phases and percentages of (a) CuO, (b) S/CuO/nGO 0.25/1, and (c) S/CuO/nGO 0.75/1

Table 1. Phase distribution and crystallinity percentages based on its diffractogram.

Sample	Phases*	χ^{2*}	% Molar CuO*	% Crystalline of CuO**
CuO	CuO	1.270	~100	45.18
S/CuO/nGO (0.25:1)	CuO	1.268	~100	31.87
S/CuO/nGO (0.50:1)	CuO	1.280	~100	31.87
S/CuO/nGO (0.75:1)	CuO, S_4, $C_{23}H_{15}N$	1.260	95	23.11
S/CuO/nGO (1.00:1)	CuO, S_{16}, $C_8H_9NO_2$	1.310	79	34.05

Notes : *) calculated using Rietica program, and **) calculated by Origin program.

Table 2. Phases in the sample.

Samples	2θ	FWHM	Crystallite Size (nm)
CuO			
CuO (monoclinic)	38.99	0.42	20.23
S/CuO/nGO (0.25:1)			
CuO (monoclinic)	38.85	0.39	21.72
S/CuO/nGO (0.50:1)			
CuO (monoclinic)	38.85	0.39	21.72
S/CuO/nG) (0.75:1)			
CuO (monoclinic)	38.77	0.61	13.90
Sulfur (S_4), orthorhombic	23.35	0.74	11.04
$C_{23}H_{15}N$, orthorhombic	24.12	0.89	9.11
S/CuO/nGO (1.00:1)			
CuO (monoclinic)	39.87	0.36	23.50
Sulfur (S_{16}), monoclinic	18.21	0.24	33.55
$C_8H_9NO_2$, monoclinic	34.93	0.24	34.73

centrifuged again using distilled water until neutral. Collected sediment dispersed in 450 mL of distilled water and sonicated for 2 h. After sonication, the ultrasonicated precipitate was dried in an oven at 60 °C to obtain GO nanosheets [27][28].

2.4. Synthesis of Nano-S/CuO/nGO

Thiourea was prepared then added CuO material, distilled water and ethanol then stirred for 1 h at room temperature. The results obtained were stored for 24 h at room temperature and calcined at 600 ºC to form S/CuO [29]. The preparation of S/CuO/nGO nanomaterials was carried out with the ratio of S/CuO and nGO weighed according to the ratio of 0.25:1 to 1.00:1. The sample was put into a 500 mL beaker and then 400 mL of distilled water was added. The sample was then ultrasonicated for 50 min so that the material and distilled water could be mixed, filtered and oven-dried until dry [29][30].

2.5. Characterization

Nano photocatalysts prepared were examined using X-ray diffraction (XRD, BTXTM III Benchtop) with Cu K_a radiation (l = 1.51406 Å, scan rate of 0.02°/s) to observe the powder crystalline structure of the photocatalysts. Fourier transform infrared spectroscopy (FTIR, *Thermo Scientific* iS5) was used to identify the functional groups existed in the crystalline structure. To know the band gap energy of the photocatalysts, UV-vis diffuse reflectance spectroscopy (Shimadzu UV-3600) is used to collect data subjecting to conversion based on the formula of Kubelka-Munk and Tauc plot [31]. Microstructure analysis was characterized using both scanning electron microscopy (SEM, Zeiss) and transmission electron microscopy (TEM, JEM-1400) to observe the morphology and topography, crystalline structure, and composition.

2.6. Antibacterial Activity Tests

The tools to be used are sterilized for 15 min in an autoclave. Glass equipment such as petri dishes and test tubes were wrapped using HVS paper which is then placed in heat-resistant plastic. Bacteria that have been grown on slanted agar media are inoculated back onto new agar media, starting with sterilization of the agar media in an autoclave. The sterilized media is poured into sterile petri dishes in the biological safety cabinet. The media was allowed to sit until it hardened, then one cycle of bacteria was taken from the slanted

agar media. Next, quadrant etching was carried out on the agar media. Then the edge of the petri dish is placed on a Bunsen, then covered with plastic wrap, incubated for 24 h in an incubator at 37 °C. Then, the bacterial colonies that grow were observed using colony counter. The antibacterial test will be carried out using 2 methods, namely: (1). the MIC method using the broth microdilution and followed by (2). the clear zone using the the Kirby-Baurer disc diffusion method. The samples to be tested are GO, CuO, S/CuO and S/CuO/nGO nanosheets. *Bacillus sp* and *E. coli* bacteria that had been cultivated on agar media were inoculated on liquid media and placed in an incubator at 37 °C for 24 h, then taken using a 0.1 µL micropipette, then swapped using a sterile cotton bat on agar media in a petri dish with adjusted environmental conditions [32][33].

2.6.1. MIC Tests

The initial step was to prepare two stock solutions; the first for the GO and CuO samples, and the second for S/CuO/nGO samples. Ten concentrations were used for both solutions, each with a difference of half the initial concentration. The futher step in the bacterial inoculation process is to prepare the nutrient broth media in a test tube that has been sterilized in an autoclave. The inoculation process begins by taking 1 oce each of *E. coli* and *Bacillus sp* bacteria and placing them in a test tube containing sterile media and then incubating for 4 h. Bacterial inoculation is carried out in laminar air flow which aims to avoid contamination during the inoculation process. Then, a treatment was carried out in test tubes and vials with a combination of 0.1 mg/mL of each each GO, CuO, S/CuO (0.25:1, 0.50:1, 0.75:1, and 1.00:1) and S/CuO/nGO (0.25:1, 0.50:1, 0.75:1, and 1.00:1) samples, 0.8 mg/mL of nutrient broth media and 0.1 mg/mL of each *E. coli* and *Bacillus sp.* bacteria. The testing process for each sample involved incubation for 24 h and observation of the samples afterward.

2.6.2. Clear Zone Tests

The MIC test results are used as a reference for the disc diffusion test. The initial preparation steps are analogous to those for the MIC test. At first, the media that has been planted with bacteria were prepared. A paper disk was took with sterile tweezers and soaked in a solution of CuO, nGO, S/CuO (each variation) and S/CuO/nGO (each variation) for each comparison as well as positive- and negative-control. The controls were placed on top of the media containing the smear of bacteria with a slight pressure so that the paper disk sticks to

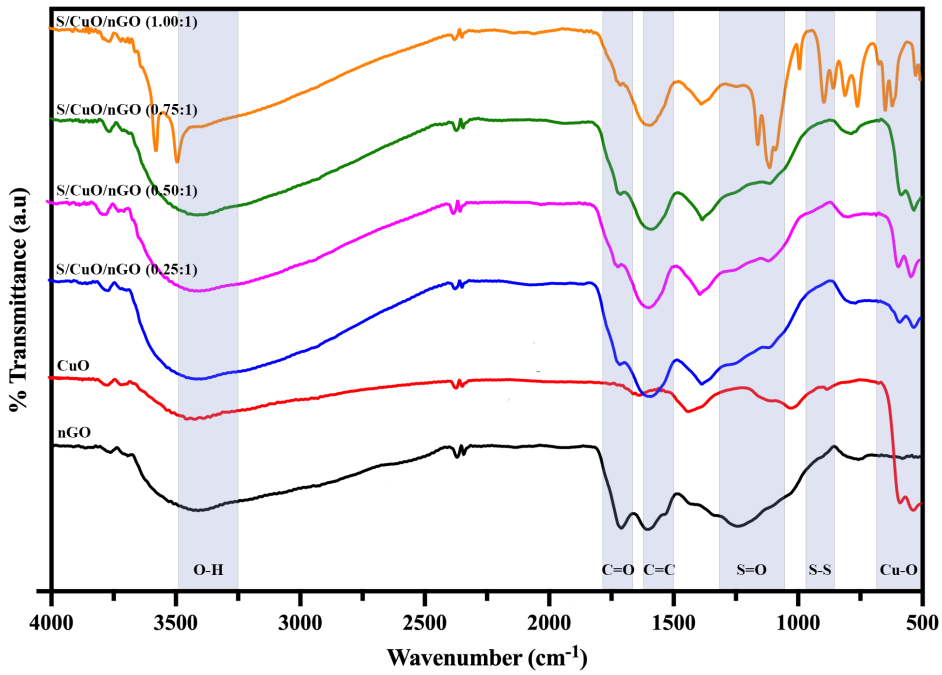

Figure 3. FTIR spectra of S/CuO/nGO in different ratio.

Table 3. A Summary of the main FTIR peaks.

Wavenumber (cm^{-1})	Functional group	References
3427.51–3446.79	O–H	[40]
1707–1710.85	C=O	[35]
1583–15836	C=C	[36]
1114–1383	S=O or SO_2	[40]
1026.13–1111	S=O	[40]
831.32–887	S–S	[38]
779.24 and 1381	C–S	[38]
754 and 786.96	C–H	[37]
480–588	S–CuO , S=O	[40]
422.42–642.30	Cu–O	[34]

the surface of the media then irradiated using visible light with varying times (15, 30, 45, 60 min). They were incubated at 37 °C for 24 h. Inhibition zone measurements were carried out after that. Antibacterial activity is declared positive if an inhibitory zone is formed in the form of a clear zone around the paper disk [33]-[36].

3. RESULTS AND DISCUSSIONS

3.1. XRD Analysis

The sample that has been prepared and characterized by XRD as shown in Figure 1, states that the main peak of CuO is at 2θ = 35.46º in accordance with JCPDS data No. 00-048-1548, and other peaks are at 2θ = 35.46, 38.66, 48.67, 53.40, 58.22, and 61.48º. The CuO crystalline phase is monoclinic and the crystalline size, based on Debye -Scherrer calculations, is 26.4 nm. The representative peak of sulfur does not appear significantly, which should be indicated at 2θ = 32.51, 46.29, and 74.96, accordance with JCPDS data on No. 00-024-1206.

This states that the sulfur is evenly distributed on S/CuO/nGO structure. The results of the monoclinic crystalline phase agreed with the results of Dehaj and Mohiabadi [37]. Furthermore, the diffractogram of S/CuO/nGO with a ratio of S/CuO to nGO of 0.25, 0.50, 0.75, and 1.00 (Figure 1) shows the diffractogram of nGO with peaks 2θ = 10.14 and 23.441°, and after impregnating S/CuO on nGO, the peak of nGO is still visible as a small bump with 2θ = 11.01°. Figure 1 shows that nGO is formed at an angle of 2θ = 23.01º showing that there are peaks at angles of 2θ = 35.54, 35.50, 38.37, 58.34, 61.57, 65.8, and 67.96º indicating the presence of a CuO crystal phase. Having impregnated by sulfur, S/CuO phase crystalline peaks showed up at 2θ = 35, 38, 48, 61, 66 and 72º and accordance with the JCPDS 01-089-2529; and 00-020-1225. The greater the concentration of S/CuO particles impregnated on the nGO surface, the smaller the nGO intensity. So, the diffractogram is dominated by the CuO crystalline phase peak, characterized by the increasing intensity of the CuO particles. Meanwhile, sulfur itself is completely dispersed with CuO so that the diffractogram peaks merge. In addition, typical peak of GO nanosheets material was also detected after impregnation with catalyst S/CuO, namely with the appearance of the peak 2θ = 11 and 23º even though it looks like bumps.

By running Rietica program in order to know how many phases formed and its crystallite sizes using Scherrer calculation, the results are shown in Figure 2 and Table 1, respectively. The Rietica's results prove that the crystalline phase formed in CuO, S/CuO/nGO for ratio 0.25:1 and 0.50:1 is only identified in one phase, namely monoclinic CuO. Meanwhile, in S/CuO/nGO with the ratio of 0.75:1 and 1.00:1 (i.e., the ratio of S/CuO to nGO), three phases were identified, namely monoclinic CuO, orthorhombic S_4, and $C_{23}H_{15}N$ compound derived from nGO, and in the ratio of 1.00:1, three phases were also identified but it was not the same at all. The phases were monoclinic CuO, monoclinic S_{16}, and monoclinic $C_8H_9NO_2$. The

Rietveld calculation results and phase distribution are presented in Table 1. The χ^2 presents that the calculation is valid if its value ≤ 4.0.

The percentage of crystalline is obtained by the ratio of the crystalline area fraction to the sum of the crystalline and amorphous area fractions. In Table 1, it can be seen that increasing the ratio of S/CuO to nGO will increase the percentage of crystalline CuO. Anomaly occurs at the S/CuO to nGO ratio of 0.75:1. This occurs because sulfur is seen to form an orthorhombic S_4 structure and nano graphene forms an orthorhombic $C_{23}H_{15}N$ structure. However, the ratio of S/CuO to nGO gives an increased crystalline percentage, amounting to 34.05%. Here, sulfur forms monoclinic S_{16} and nano graphene forms monoclinic $C_8H_9NO_2$ structures. In Table 2, the crystallite size is determined based on the Scherrer equation. It can be seen that increasing the ratio of S/CuO to nGO, especially at a ratio of 0.75:1 gives a crystallite size of 13.90 nm, which is relatively smaller than CuO and the ratios of 0.25:1 and 0.50:1 for S/CuO/nGO. Then, the crystallite size increases to 23.50 nm when the ratio of S/CuO/nGO becomes 1.00:1.

3.2. FTIR Analysis

The S/CuO/nGO material is then analyzed using FTIR spectroscopy to produces peaks in the IR spectrum, namely at wavenumbers 3389 to 3572 cm $^{-1}$ indicates the presence of O–H stretching vibrations. The stretching vibration of the C=O in either carboxyl or carbonyl functional group is observed at a wavenumber of 1707 up to 1710 cm^{-1} [35], and the wavenumber 1585–1583 cm^{-1} shows C=C bond [36]. Then, the presence of C–H bonds is presented by 754 and 787 cm^{-1} [37]. The vibration of Cu–O bonds is shown by peaks existing at wavenumber of 422 to 642 cm^{-1} [34]. Figure 3 shows that there is a shift in the clusters formed, this is due to differences variations are carried out resulting in increasingly strong shifts. For the C–S sulfur bond itself, it can be seen in the numbers of each variation 0.50:1, 1.00:1 is 1381 cm^{-1} [38]. Gul and Alrobei reported the C=C group appeared at 1581 cm^{-1} [39].

The spectrum of the S/CuO catalyst identified

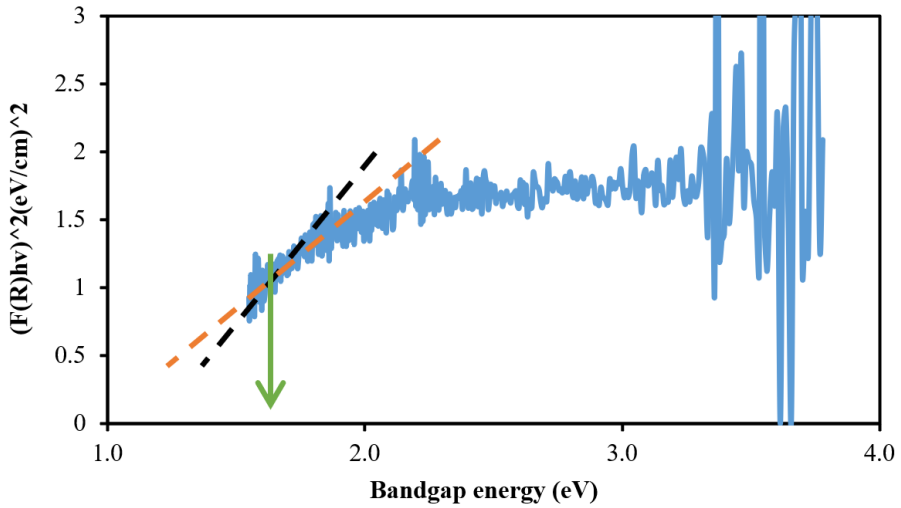

Figure 4. Determination of band gap energy for S/CuO/nGO (0.50:1).

Table 4. Bandgap energy (E_{bg}).

Samples	E_{bg} (eV)
nGO	~2.00
CuO	1.75
S/CuO/nGO (0.25:1)	1.50
S/CuO/nGO (0.50:1)	1.60
S/CuO/nGO (0.75:1)	1.42
S/CuO/nGO (1.00:1)	1.40

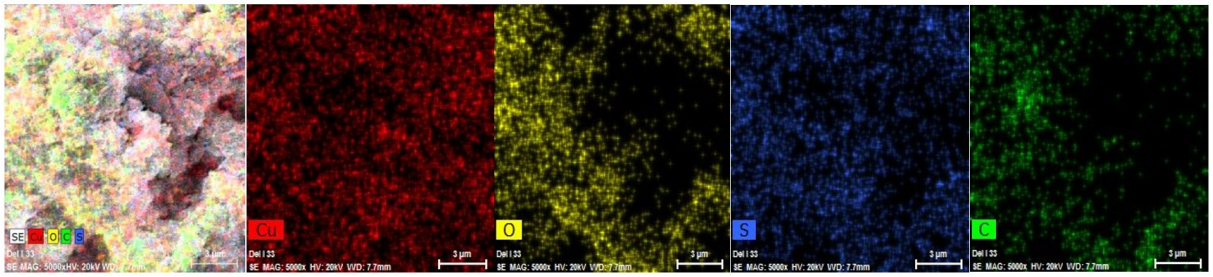

Figure 5. SEM micrographs of S/CuO/nGO (1.00:1) in the left, and others are presenting the element of Cu (red), O (yellow), S (blue), and C (green). Operational condition : SE MAG 5000×, HV 20 kV, and WD 7.6 mm.

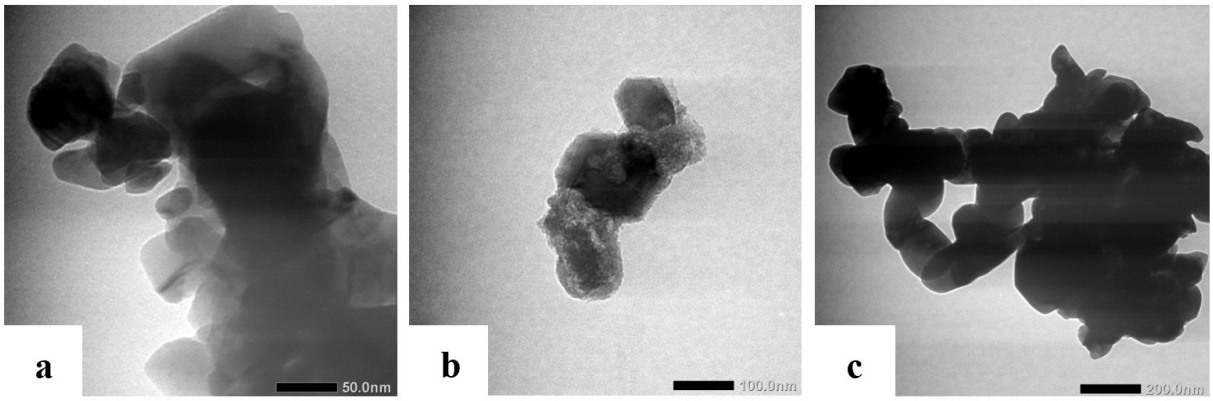

Figure 6. TE-micrograph of S/CuO at (a) 50 nm, Mag. 80k ; (b) 100 nm, Mag. 40k; and (c) 200nm, Mag. 20k with the accel. 120 V.

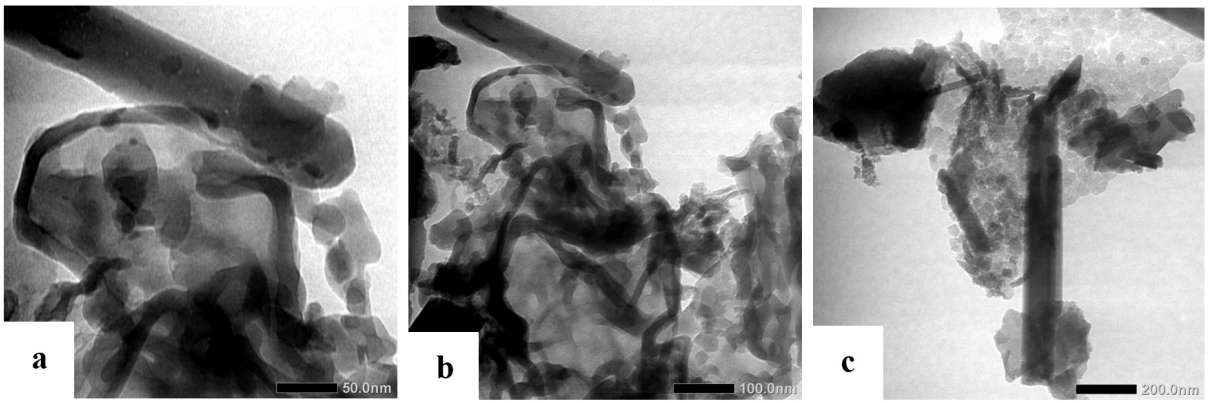

Figure 7. TEM micrograph of S/CuO/nGO (1:1) at (a) 50 nm, Mag. 80k ; (b) 100 nm, Mag. 40k; and (c) 200 nm; Mag. 20k with the accel. 120 V.

from the results of nanomaterial analysis, and S/CuO/nGO appears several characteristic transmittance peaks in the wavenumber range of 1381, 1111, and 588–480 cm^{-1} which indicate the presence of stretching and bending vibrations in the S=O and S–CuO bonds, respectively [40]. The difference in transmittance peaks' appearance in all the S/CuO/nGO catalysts' variations can be implied due to the effect of varying amounts of sulfur doped on the CuO so that affects the transmittance peak results. The stretching vibration of S–S bond at wave number of 887 cm^{-1} is more pronounced at the ratio of S/CuO to nGO equals to 1.00:1 than at other ratios. The same is found for C–S bending and stretching vibrations. This phenomenon can be implied that sulfur is not only bound to Cu metal, but also to nGO and to sulfur of another compound. The presence of vibrations from C–C and C–H bonds, which appear at wavenumbers of 1587 and 758 cm^{-1}, respectively, indicates that these

vibrations originate from GO. The vibration peaks that arise from the bonds owned by S/CuO/nGO nano composites prepared are shown in Table 3.

3.3. Band Gap Energy Analysis

Determination of the band gap energy value using the Tauc plot [31] is displayed graphically as an example in Figure 4. All other band gap energy determinations of varied S/CuO/nGO nano composites are presented in Table 4. It can be seen that the band gap energy for samples varies with the ratio of S/CuO to nGO in the range of 0.25, 0.50, 0.75, and 1.00 is significantly different. This difference is due to differences in the S/CuO content in nGO where increasing levels cause the band gap energy value to decrease if you look at the respective band gap energies of CuO and nGO, namely 1.75 and 2.0 eV. The band gap energy decreases to 1.4–1.6 eV as the ratio of S/CuO to nGO increases. The phenomenon of decreasing band gap energy implies that there is a bonding interaction between sulfur, CuO and nGO.

Then, band gap value of each nanomaterial of S/CuO/nGO is a variation of 0.25:1 of 1.5 eV while a variation of 0.75:1 is 1.6 eV. The band gap energy results obtained are compared with the band gap of CuO which is one of the components of the S/CuO catalyst is located in the range 1.2–1.9 eV [41]. This can be concluded that there is an influence of the amount of S/CuO variation to nGO in the composites of S/CuO/nGO catalyst on the band gap energy value. The greater the amount of S/CuO in nGO, the smaller the band gap energy value obtained. The band-gap energy value indicates potential as a photocatalyst. The band-gap energy of the S/CuO/nGO nanomaterial is in the range of 1.4–1.5 eV, meaning that the sample can work under UV and visible light [42].

3.4. Microstructure Analysis

3.4.1. SEM Analysis

If we focus on the SEM distribution results for each element such as Cu, O, and S and C; it can be seen that CuO material covers the surface of the nGO material [43][44], although in certain locations and limited, dark areas, indicating that CuO has infiltrated the inner layer of nGO. The pattern shown by the elements oxygen and sulfur also states that S in CuO is in the inner layer of nGO. Furthermore, element C which represents nGO appears brighter in color at certain locations, which indicates that nGO is at the certain surface of the material. This can be seen in the leftmost image. Therefore, in Figure 5, it is shown that sulfur and CuO are well distributed on nano graphene oxides representing by the element of both oxygen and carbon.

3.4.2.TEM Analysis

The TE-micrograph result of the S/CuO nanomaterial are presented in Figure 6. In the results of a special TE-micrograph at a scale of 200 nm (c), it is clear that CuO is in a monoclinic form

Table 5. Minimum inhibitory concentratin (MIC).

Samples	MIC (mg/mL)	
	E. coli	***B. subtillis***
CuO	0.256	4.096
nGO	2.048	2.048
S/CuO (0.25:1)	0.16	0.01
S/CuO (0.50:1)	0.08	0.16
S/CuO (0.75:1)	0.04	0.00125
S/CuO (1.00:1)	0.04	0.08
S/CuO/nGO (0.25:1)	0.08	0.05
S/CuO/nGO (0.50:1)	0.01	0.08
S/CuO/nGO (0.75:1)	0.01	0.00125
S/CuO/nGO (1.00:1)	0.01	0.004

Table 6. Clear zone analysis data against *E. coli* bacteria.

Sample	Formed clear zone (mm) at the exposure time				
	0 min	15 min	30 min	45 min	60 min
Streptomycin (+)	20	20	20	20	20
nGO	1	1	1	1	1
CuO	2	2	1	1	1
S/CuO (0.25:1)	2	3	4	3	2
S/CuO (0.50:1)	3	5	3	4	4
S/CuO (0.75:1)	3	6	5	6	4
S/CuO (1.00:1)	5	10	8	6	5
S/CuO/nGO (0.25:1)	3	7	6	9	6
S/CuO/nGO (0.50:1)	3	8	7	8	6
S/CuO/nGO (0.75:1)	4	10	8	6	7
S/CuO/nGO (1.00:1)	4	12	10	9	8

Table 6. Clear zone analysis data against *B. subtillis* bacteria.

Sample	Formed clear zone (mm) at the exposure time				
	0 min	15 min	30 min	45 min	60 min
Streptomycin (+)	20	20	20	20	20
nGO	3	3	5	5	5
CuO	3	3	5	5	5
S/CuO (0.25:1)	3	4	4	3	4
S/CuO (0.50:1)	4	4	4.5	4.5	4
S/CuO (0.75:1)	4	5	6	5	5
S/CuO (1.00:1)	5	5	8	5	6
S/CuO/nGO (0.25:1)	4	6	8	6	8
S/CuO/nGO (0.50:1)	3	7	9	7	9
S/CuO/nGO (0.75:1)	4	8	14	10	8
S/CuO/nGO (1.00:1)	3	10	18	14	12

that combines with each other. So that it forms a fairly long chain. At this scale, sulfur is not clearly visible, only a dark blanket and spherical shape. However, if you look at the TEM results at a scale of 100 nm (b), you can see CuO monoclinic covered in sulfur which is shaped like a sphere [45] [46]. The sulfur surrounds the surface of CuO quite evenly. Furthermore, At the 50 nm scale of CuO (a, left), a combination of large monoclinic CuO and fragmented monoclinic CuO on the sides is visible. However, it appears that sulfur still covers it (dark and white colored).

In Figure 7, it can be seen that the CuO structure, as shown in Figure 6, is a combination of monoclinic phases such as tubes and chains. Next is dark colored sulfur, which also surrounds CuO, spherical shape surrounds the CuO structure [46]. Nano GO, more visible in Figure 6(c), is a spherical grain covering the S/CuO. The nGO that is formed is not all crystalline as explained in the XRD data, so there is a possibility that there is still graphite, graphene remaining and the layer is not even a single layer. In Figures 7(a) and 7(b), you can see a black ribbon-like coil. This allows the presence of nGO chains or tubes' possibility [47][48]. Overall the phase size is still on the nano scale.

3.5. Antibacterial Activity of Photocatalysts

The antibacterial activity test was carried out using the MIC and disk diffusion methods. The samples to be tested are GO, CuO nanosheets, S/CuO catalyst and S/CuO/nGO nanomaterials. The MIC test is carried out to determine the minimum inhibitory concentration of the sample tested. The results obtained from the MIC test can be seen in Table 5. It showed that the GO and CuO nanosheets samples have sensitivity to bacteria in the concentration range of 0.2–4.0 mg/mL. This is similar to the research of another group, where CuO sensitivity appears in the range of 2–10 mg/mL [49]. The CuO doped with sulfur has an increase activity, namely the appearance of a lower MIC value, at the concentration range 0.000125–0.160000 mg/mL. In addition, sulfur has an influence on antibacterial activity at the MIC of 1.024 mg/mL [50]. Therefore, it can be concluded that the addition of sulfur into CuO ameliorates its activity as an antibacterial agent.

The influence of sulfur was also confirmed in the overall MIC test results, those samples with good MIC values were obtained for S/CuO and S/CuO/nGO samples with a concentration range of 0.00125–0.00400 mg/mL. This phenomenon emphasizes that the addition of sulfur in larger quantities will increase its antibacterial activity with minimum inhibitory concentrations, for both types of bacteria, Gram-positive and Gram-negative. However, if the data in Table 5 is observed more closely, the S/CuO/nGO nanomaterial has a better impact on *Bacillus sp* than on *E. coli*.

In the Kirby-Bauer disc diffusion results as shown in Table 6, the optimum exposure time giving the best clear zone is at 15 min for *E. coli*, and 30 min for *B. subtilis*. The inhibition zone formed for S/CuO and S/CuO/nGO is greater in *E. coli* than in *B. subtilis* bacteria. The zone formed is not too large, this is due to the concentration of the sample used which is relatively small. The previous research was conducted by Bousiakou et al., the clear zone obtained is 0.11 to 0.31 mm for *Staphylococcus aureus*, *E. coli* and *Pseudomonas aeruginosa* bacteria [51]. These results are due to the concentration of nGO used, in the range of 0.25 to 1.50 mg/mL [51]. Furthermore, the best result of this research is shown in the ratio of S/CuO to nGO 1:1 where the clear zone is 12 and 18 mm for *E. coli* (Table 6) and *B. subtilis* (Table 7), respectively. It seems that the antibacterial activity in *B. subtilis* is greater than that in *E. coli*. In addition, the initial test without visible light irradiation, each material as an antibacterial agent, had a clear zone in the range of 2–3 mm. From the Tables 6 and 7, the minimum concentration used for the clear zone test is 0.00125 mg/mL and is in accordance with the test carried out by Hajipour et al. [49] with results for Gram-positive bacteria of 4.5–13 mm, while Gram-negative bacteria were in the range of 3–11 mm.

In general, antibacterial activity in Gram-negative bacteria (*E. coli*) has a smaller inhibition zone diameter than that in Gram-positive bacteria (*Bacillus sp*). These different results are due to differences in the cell wall structure of the two bacteria, where Gram-negative bacteria are more complex than Gram-positive bacteria. In more detail, Gram-negative bacteria have a cell wall

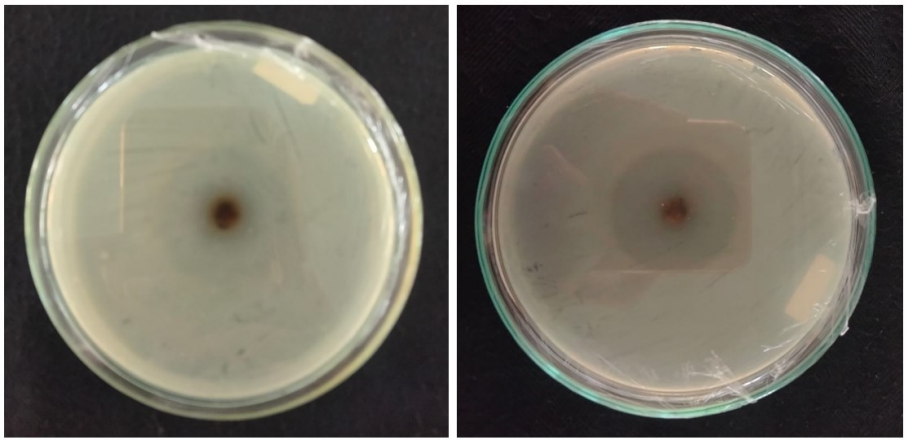

Figure 8. Clear zone of S/CuO/nGO (1.00:1) against *E. coli* (left) is 12 mm and *B. substilis* (right) is 18 mm.

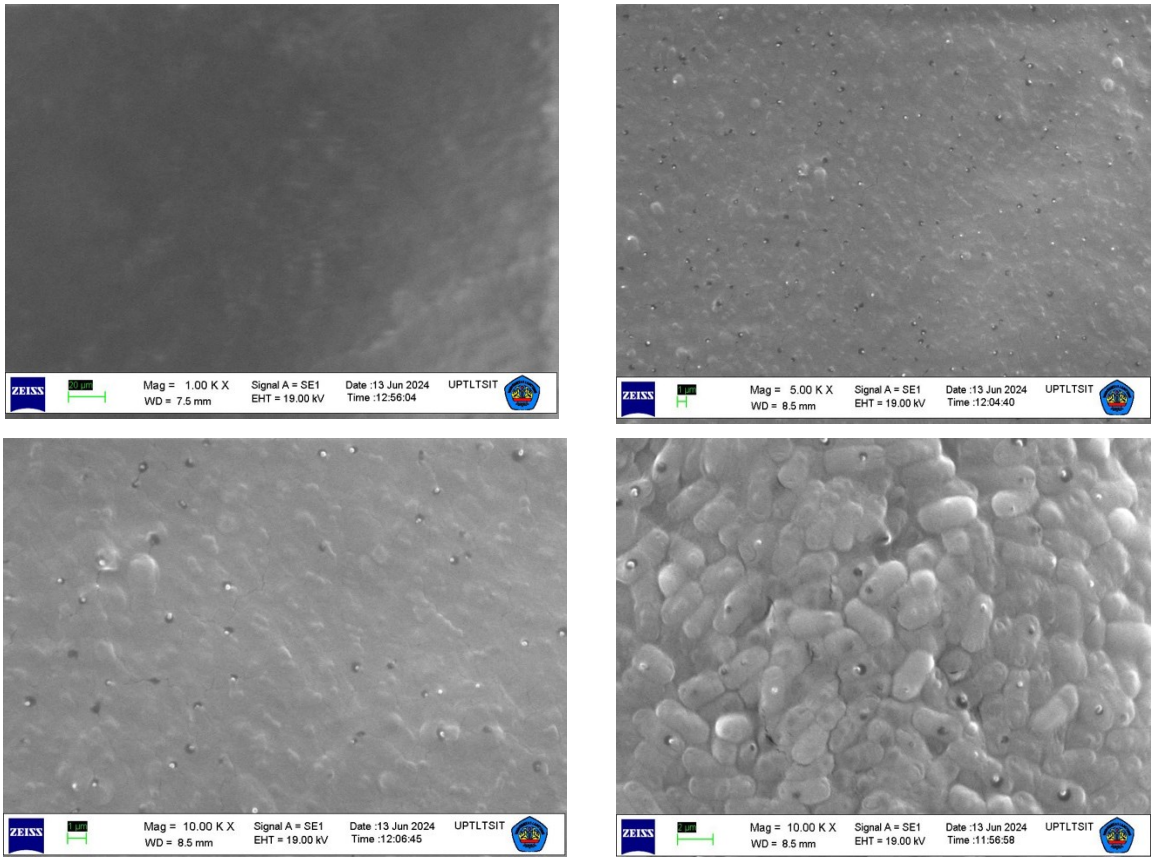

E. coli *B. subtilis*

Figure 9. SEM-micrographs of *E. coli* and *B. subtillis* after exposure to visible light.

consisting of 3 layers, which are, the outer layer, the middle layer and the inner layer. However, Gram-positive bacteria only have a single layer in their cell walls. If looking at the photocatalytic activity of both S/CuO and S/CuO/nGO at each ratio, it appears that the more sulfur added to each CuO and nGO has relatively better antibacterial activity. In case of S/CuO, the bacterial activity is in the range 4 through 8 mm in 30 min exposure. Then, for S/CuO/nGO, the bacterial activity increases from 8 to 18 mm as shown in Table 7.

In the visualization in the range of the clear zone at the border and the outer zone next to border, as shown in Figure 9, SEM results show that the *E. coli* and *B. subtilis* bacteria look damaged (the cell wall was broken, a black appearance) in both the inner and outer boundary zones. The appearance of black-marks on the bacteria indicates that the S/CuO/nGO material with various ratios is able to kill the bacteria by damaging its cell membranes. This can be explained through the following mechanisms. As known, the CuO NP is active as antibacterial by destroying bacterial cell membranes through ROS [52]. Apart from that, nGO which turns out to be active as antibacterial, is capable of damaging through the mechanism of electrons withdraw from inside the membrane cell [53]. In the recent research of the Baek group [21] using a TiO_2-CuO@GO hybrid catalyst was able to eliminate bacteria through a mix mechanism of both ROS and disruption of cell membrane self-protection. Therefore, by indirect think, the S/CuO/nGO nano composites can be implied that is able to damage cell membranes of bacteria by the release of metal cations, the emergence of ROS, and inhibiting biofilm formation of the bacteria [21][54]-[56].

4. CONCLUSIONS

The study demonstrated that the S/CuO/nGO composite nanomaterials were successfully synthesized, as confirmed by FTIR, XRD, DRS, SEM, TEM, and elemental mapping analyses, and exhibited significant antibacterial activity. Among the tested compositions, the S/CuO/nGO

nanomaterial with a 1.00:1 ratio showed the highest efficacy, inhibiting *E. coli* and *B. subtilis* with clear zones of 12 and 18 mm, respectively, and demonstrating very low MIC (0.01 mg/mL for *E. coli* and 0.00125 mg/mL for *B. subtilis*). SEM observations further revealed that bacterial cell membranes were visibly damaged at the boundaries of inhibition zones, confirming the nanomaterial's potent antibacterial mechanism. These findings imply that S/CuO/nGO nanocomposites, particularly at ratios of 0.75:1 and 1.00:1, hold great potential for applications in antibacterial coatings and surface protection. Future research could explore long-term stability, cytotoxicity, and practical implementation of these nanocomposites in medical or industrial coating systems to optimize safety and effectiveness.

AUTHOR INFORMATION

Corresponding Authors

Rudy T. M. Situmeang — Department of Chemistry, University of Lampung, Bandar Lampung-35141 (Indonesia);
orcid.org/0000-0001-6622-0362
Email: rudy.tahan@fmipa.unila.ac.id

Jarnuzi Ganlazuardi — Department of Chemistry, University of Indonesia, Kota Depok -16424 (Indonesia);
orcid.org/0000-0001-5991-7110
Email: jarnuzi@ui.ac.id

Authors

Sumardi Sumardi — Department of Biology, University of Lampung, Bandar Lampung-35141 (Indonesia);
orcid.org/0000-0002-2773-7083

Syangap Diningrat Sitompul — Department of Chemistry, University of Lampung, Bandar Lampung-35141 (Indonesia);
orcid.org/0009-0008-3663-1310

Aniska Legia — Department of Chemistry, University of Lampung, Bandar Lampung-35141 (Indonesia);
orcid.org/0009-0008-8230-4986

Tri Umiana Soleha — Faculty of Medicine, University of Lampung, Bandar Lampung-35141 (Indonesia);
orcid.org/0009-0009-5414-0416

Ni Luh Gede Ratna Juliasih — Department of Chemistry, University of Lampung, Bandar Lampung-35141 (Indonesia);
orcid.org/0000-0002-6202-461X

Author Contributions

Conceptualization, R. T. M. S. and J. G.; Methodology, R. T. M. S., J. G., and S. S.; Software, S. D. S., A. L., and R. T. M. S.; Formal Analysis, R. T. M. S., S. S., T. U. S., N. L. G. R. J.; Resources, R. T. M. S., J. G.; Writing – Original Draft Preparation, R. T. M. S.; Writing – Review & Editing, R. T. M. S. and J. G.; Supervision, R. T. M. S.; Funding Acquisition, N. L. G. R. J., and T. U. S.

Conflicts of Interest

The authors declare no conflict of interest.

ACKNOWLEDGEMENT

This research is supported by the Research Innovation and Collaboration Batch 3 Domestic Program at the Higher Education for Technology and Innovation (HETI) ADB Loan Project [Grant Number: 4110-INO] through the Competitive Research Grant of Univeristy of Lampung, with research contract No. 235/UN26/HK.01.03/2024.

DECLARATION OF GENERATIVE AI

During the preparation of this work, the author(s) used authentic QuillBot with a premium subscription to correct grammar and paraphrase some statements in the properly cited references. After using this tool/service, the author(s) reviewed and edited the content as needed and will take full responsibility for the content of the publication.

REFERENCES

[1] R. Mithuna, R. Tharanyalakshmi, I. Jain, S. Singhal, D. Sikarwar, and S. Das. (2024). "Emergence of antibiotic resistance due to the excessive use of antibiotics in medicines and feed additives: A global scenario with emphasis on the Indian perspective". *Emerging Contaminants.* **10** : 100389. 10.1016/j.emcon.2024.100389.

[2] S. Raghavan and K. S. Kim. (2024). "Host immunomodulation strategies to combat pandemic-associated antimicrobial-resistant secondary bacterial infections". *International Journal of Antimicrobial Agents.* **64** (4): 107308. 10.1016/j.ijantimicag.2024.107308.

[3] M. L. Tummino, E. Laurenti, P. Bracco, C. Cecone, V. La Parola, C. Vineis, and M. L. Testa. (2023). "Antibacterial properties of functionalized cellulose extracted from deproteinized soybean hulls". *Cellulose.* **30** : 7805-7824. 10.1007/s10570-023-05339-w.

[4] M. P. Romero, V. S. Marangoni, C. G. de Faria, I. S. Leite, C. de Carvalho Castro e Silva, C. M. Maroneze, M. A. Pereira-da-Silva, V. S. Bagnato, and N. M. Inada. (2020). "Graphene oxide mediated broad-spectrum antibacterial based on bimodal action of photodynamic and photothermal effects". *Frontiers in Microbiology.* **10** : 2995. 10.3389/fmicb.2019.02995.

[5] F. Eskandari, Y. Ghahramani, A. Abbaszadegan, and A. Gholami. (2023). "The antimicrobial efficacy of nanographene and double antibiotic paste per se and in combination: Part II". *BMC Oral Health.* **23** : 253. 10.1186/s12903-023-02957-5.

[6] D. Singh, D. Jain, D. Rajpurohit, G. Jat, H. Singh-Kushwaha, A. Singh, S. R. Mohanty, M. K. Al-Sadoon, W. Zaman, and S. K. Upadhyay. (2023). "Bacteria assisted green synthesis of copper oxide nanoparticles and their potential applications as antimicrobial agents and plant growth stimulants". *Frontiers in Chemistry.* **11** : 1154128. 10.3389/fchem.2023.1154128.

[7] D. Rivera-Mendoza, A. R. Vilchis-Nestor, K. Juarez-Moreno, E. Castro-Longoria, and K. M. Flores-Rábago. (2023). "Antibacterial activity of biosynthesized copper oxide nanoparticles (CuO NPs) using Ganoderma sessile". *Antibiotics.* **12** : 1251. 10.3390/antibiotics12081251.

[8] T. Hesabizadeh, K. Sung, M. Park, S. Foley, A. Paredes, S. Blissett, and G. Guisbiers. (2023). "Synthesis of antibacterial copper oxide nanoparticles by pulsed laser ablation in liquids: Potential application against foodborne pathogens". *Nanomaterials.* **13** : 2206. 10.3390/nano13152206.

[9] F. A. Bezza, S. M. Tichapondwa, and E. M. N. Chirwa. (2020). "Fabrication of monodispersed copper oxide nanoparticles with potential application as antimicrobial agents". *Scientific Reports.* **10** : 16680. 10.1038/s41598-020-73497-z.

[10] R. B. Asamoah, E. Annan, B. Mensah, P. Nbelayim, V. Apalangya, B. Onwona-Agyeman, and A. Yaya. (2020). "A comparative study of antibacterial activity of CuO/Ag and ZnO/Ag nanocomposites". *Advances in Materials Science and Engineering.* **2020** : 7814324. 10.1155/2020/7814324.

[11] S. Zheng, W. Chen, C. Shi, and J. Han. (2023). "Thermostable ZnO/Ag@SiO2 nanohybrid material for extraordinary antibacterial activity polyester fibers". *Polymer Engineering and Science.* **64** (1): 386-398. 10.1002/pen.26555.

[12] R. Gallegos-Monterrosa, R. O. Mendiola, Y. Nuñez, C. Auvynet, K. M. Kumar, B. Tang, L. I. Ruiz-Ortega, and V. H. Bustamante. (2023). "Antibacterial and antibiofilm activities of ZIF-67". *The Journal of Antibiotics.* **76** : 603-612. 10.1038/s41429-023-00637-8.

[13] D. Han, X. Liu, and S. Wu. (2022). "Metal-organic framework-based antibacterial agents and their underlying mechanisms". *Chemical Society Reviews.* **51** : 7138-7169. 10.1039/D2CS00460G.

[14] Y. Zhang, S. Cheng, H. Jia, J. Zhou, J. Xi, J. Wang, X. Chen, and L. Wu. (2023). "Green synthesis of platinum nanoparticles by Nymphaea tetragona flower extract and their skin lightening, antiaging effects". *Arabian Journal of Chemistry.* **16** : 104391. 10.1016/j.arabjc.2022.104391.

[15] M. Zou, M. Du, M. Zhang, T. Yang, H. Zu, P. Wang, and S. Bao. (2015). "Synthesis and deposition of ultrafine noble metallic nanoparticles on amino-functionalized halloysite nanotubes and their catalytic application". *Materials Research Bulletin.* **61** : 375-382. 10.1016/j.materresbull.2014.10.053.

[16] B. Meesaragandla, S. Hayet, T. Fine, U. Janke, L. Chai, and M. Delcea. (2022). "Inhibitory effect of epigallocatechin gallate-silver nanoparticles and their lysozyme bioconjugates on biofilm formation and cytotoxicity". *ACS Applied Bio Materials.* **5** : 4213-4221. 10.1021/acsabm.2c00409.

[17] M. Fahim, A. Shahzaib, N. Nishat, A. Jahan, T. A. Bhat, and A. Inam. (2024). "Green synthesis of silver nanoparticles: A comprehensive review of methods, influencing factors, and applications". *JCIS Open.* **16** : 100125. 10.1016/j.jciso.2024.100125.

[18] F. Momtaz, E. Momtaz, M. A. Mehgardi, M. Momtaz, T. Narimani, and F. Poursina. (2024). "Enhanced antibacterial properties of polyvinyl alcohol/starch/chitosan films with NiO-CuO NPs for food packaging". *Scientific Reports.* **14** : 7356. 10.1038/s41598-024-58210-8.

[19] M. Li, Z. Chen, L. Yang, J. Li, J. Xu, C. Chen, Q. Wu, M. Yang, and T. Liu. (2022). "Antibacterial activity and mechanism of GO/Cu2O/ZnO coating on ultrafine glass fiber". *Nanomaterials.* **12** : 1857. 10.3390/nano12111857.

[20] B. A. Omran, M. O. Abdel-Salam, H. H. Farghal, M. M. H. El-Sayed, and K. H. Baek. (2025). "Myco-architecture of proficient antibacterial CuO/Ag2O-grafted graphene oxide nanoconjugates: Characterization and Congo red degradation-assisted by the activation of peroxymonosulfate". *Materials Research Bulletin.* **190** : 113496. 10.1016/j.materresbull.2025.113496.

[21] B. A. Omran, M. O. Abdel-Salam, H. H. Farghal, M. M. H. El-Sayed, and K. H. Bek. (2025). "Synthesis of TiO2-CuO@graphene oxide hybrid bionanocomposite with enhanced antibacterial and organic dye degradation activities". *Materials Advances.* **6** : 2654. 10.1039/D5MA00031A.

[22] M. D. Rojas-Andrade, G. Chata, D. Rouholiman, J. Liu, C. Saltikov, and S. Chen. (2017). "Antibacterial mechanisms of graphene-based composite nanomaterials". *Nanoscale.* **9** : 994-1006. 10.1039/C6NR08733G.

[23] Y. H. Kim, G. H. Kim, K. S. Yoon, S. Shankar, and J. W. Rhim. (2020). "Comparative antibacterial and antifungal activities of sulfur nanoparticles capped with chitosan". *Microbial Pathogenesis.* **144** : 104178. 10.1016/j.micpath.2020.104178.

[24] F. Tariq, R. Hussain, Z. Noreen, A. Javed, A. Shah, A. Mahmood, M. Sajjad, H. Bokhari, and S. ur Rahman. (2022). "Enhanced antibacterial activity of visible light activated sulfur-doped TiO2 nanoparticles against Vibrio cholerae". *Materials Science in Semiconductor Processing.* **147** : 106731. 10.1016/j.mssp.2022.106731.

[25] R. Situmeang and R. Djayasinga. (2015). "Preparation and characterization of nanosize spinel Ni0.9Fe2Cu0.1O4 using pectin as binding agent. **1** : 48-55.

[26] K. Yazhini and S. K. Suja. (2019). "Synthesis and characterization of hetero-metal oxide nano-hybrid composite on pectin scaffold". *Applied Surface Science.* **491**. 10.1016/j.apsusc.2019.06.150.

[27] S. Ying, Z. Guan, P. C. Ofoegbu, P. Clubb, C. Rico, F. He, and J. Hong. (2022). "Green synthesis of nanoparticles: Current developments and limitations". *Environmental Technology & Innovation.* **26**. 10.1016/j.eti.2022.102336.

[28] H. Sharma and S. Mondal. (2020). "Functionalized graphene oxide for chemotherapeutic drug delivery and cancer treatment: A promising material in nanomedicine". *International Journal of Molecular Sciences.* **21**. 10.3390/ijms21176280.

[29] T. Ohno, M. Akiyoshi, T. Umebayashi, K. Asai, T. Mitsui, and M. Matsumura. (2004). "Preparation of S-doped TiO2 photocatalyst and their photocatalytic activities under visible light irradiation". *Journal of Photochemistry and Photobiology A: Chemistry.* **162** (1). 10.1016/j.jphotochem.2004.01.007.

[30] F. Anjum, M. Shaban, M. Ismail, S. Gul, E. M. Bakhs, M. A. Khan, U. Sharafat, S. B. Khan, and M. I. Khan. (2023). "Novel synthesis of CuO/GO nanocomposites and their photocatalytic potential in the

degradation of hazardous industrial effluents". *ACS Omega.* **8**. 10.1021/acsomega.3c00129.

[31] R. Situmeang, R. Romiyati, S. D. Yuwono, P. Manurung, I. Firdaus, and S. Sembiring. (2022). "The effect of vanadium addition in Ni1-xVxFe2O4 nano photocatalysts on Remazol golden yellow degradation under visible light irradiation". *Advances in Natural Sciences: Nanoscience and Nanotechnology.* **13** (3). 10.1088/2043-6262/ac8d8f.

[32] R. Biermann and S. Beutel. (2023). "Endospore production of Bacillus spp. for industrial use". *Engineering in Life Sciences.* **23**. 10.1002/elsc.202300013.

[33] K. L. Elbing and R. Brent. (2019). "Recipes and Tools for Culture of Escherichia coli". *Current Protocols in Molecular Biology.* **125** (1): e83. 10.1002/cpmb.83.

[34] A. Fatiqin, H. Amrulloh, and W. Simanjuntak. (2021). "Green synthesis of MgO nanoparticles using Moringa oleifera leaf aqueous extract for antibacterial activity". *Bulletin of the Chemical Society of Ethiopia.* **35** (1): 161-170. 10.4314/bcse.v35i1.14.

[35] M. Balouiri, M. Sadiki, and S. K. Ibnsouda. (2016). "Methods for in vitro evaluating antimicrobial activity: A review". *Journal of Pharmaceutical Analysis.* **6** (2). 10.1016/j.jpha.2015.11.005.

[36] B. Kebede and W. Shibeshi. (2022). "In vitro antibacterial and antifungal activities of extracts and fractions of leaves of Ricinus communis Linn against selected pathogens". *Veterinary Medicine and Science.* **8**. 10.1002/vms3.772.

[37] M. S. Dehaj and M. Z. Mohiabadi. (2019). "Experimental study of water-based CuO nanofluid flow in heat pipe solar collector". *Journal of Thermal Analysis and Calorimetry.* 10.1007/s10973-019-08046-6.

[38] K. Krishnamoorthy, M. Veerapandian, K. Yun, and S. J. Kim. (2013). "The chemical and structural analysis of graphene oxide with different degrees of oxidation". *Carbon.* **53**. 10.1016/j.carbon.2012.10.013.

[39] W. Gul and H. Alrobei. (2021). "Effect of graphene oxide nanoparticles on the physical and mechanical properties of medium density fiberboard". *Polymers.* **13** (11). 10.3390/polym13111818.

[40] B. Paulchamy, G. Arthi, and B. D. Lignesh. (2015). "A simple approach to stepwise synthesis of graphene oxide nanomaterial". *Journal of Nanomedicine & Nanotechnology.* **6**. 10.4172/2157-7439.1000253.

[41] A. Kotbi, M. Lejeune, P. Barroy, I. H. Alaoui, A. Zeinert, and M. Jouiad. (2025). "High photovoltaic performance of a p-CuO/n-Si heterojunction prepared by a simple fabrication method". *Journal of Sol-Gel Science and Technology.* **114** (3). 10.1007/s10971-025-06699-4.

[42] T. M. Palanivel, N. Shivakumar, A. Al-Ansari, and R. Victor. (2020). "Bioremediation of copper by active cells of Pseudomonas stutzeri LA3 isolated from an abandoned copper mine soil". *Journal of Environmental Management.* **253**. 10.1016/j.jenvman.2019.109706.

[43] A. Gholami, F. Emadi, A. Amini, M. Shokripour, M. Chashmpoosh, and N. Omidifar. (2020). "Functionalization of graphene oxide nanosheets can reduce their cytotoxicity to dental pulp stem cells". *Journal of Nanomaterials.* **2020**. 10.1155/2020/6942707.

[44] K. Ungeuer, K. W. Marzalek, M. Mitura-Nowak, M. Perzanowski, P. Jelen, M. Marzalek, and M. Sitarz. (2022). "Influence of Cr ion implantation on physical properties of CuO thin films". *International Journal of Molecular Sciences.* **23** (9). 10.3390/ijms23094541.

[45] M. Sulaiman, M. Al-Masri, A. Al Ali, D. Aref, A. Hussein, I. Saadeddin, and I. Warad. (2015). "Synthesis of nano-sized sulfur nanoparticles and their antibacterial activities". *Journal of Materials and Environmental Sciences.* **6** (2).

[46] S. Haseki, Y. Kucukcobanoglu, M. Ayisigi, T. Oztekin, and L. Y. Aktas. (2025). "Influence of synthesis method on physicochemical properties and antibacterial activity of green synthesized CuO nanoparticles from Laurus nobilis L. leaf

extracts". *Plant Nanobiology.* **11**. 10.1016/j.plana.2024.100128.

[47] W. Srihata, T. Jamnongkan, U. Rattanasak, S. Boonsang, and S. Kaewpirom. (2017). "Enhanced electrostatic dissipative properties of chitosan/gelatin composite filled with reduced graphene oxide". *Journal of Materials Science: Materials in Electronics.* **28** (1). 10.1007/s10854-016-5620-0.

[48] M. H. Nawaz, J. Xu, Z. Song, S. Riaz, D. Han, and L. Niu. (2019). "N-doped graphene oxide decorated with PtCo nanoparticles for immobilization of double-stranded deoxyribonucleic acid and investigation of clenbuterol-induced DNA damage". *ACS Omega.* **4**. 10.1021/acsomega.9b02184.

[49] P. Hajipour, A. Bahrami, A. Eslami, and A. Hosseini-Abari. (2020). "Chemical bath synthesis of CuO–GO–Ag nanocomposites with enhanced antibacterial properties". *Journal of Alloys and Compounds.* **821**. 10.1016/j.jallcom.2019.153456.

[50] S. Saedi, M. Shokri, and J. W. Rhim. (2020). "Antimicrobial activity of sulfur nanoparticles: Effect of preparation methods". *Arabian Journal of Chemistry.* **13** (8). 10.1016/j.arabjc.2020.06.014.

[51] L. G. Bousiakou, L. Qindeel, O. M. Al-Dossary, and K. Helen. (2022). "Synthesis and characterization of graphene oxide (GO) sheet for pathogen inhibition: Escherichia coli, Staphylococcus aureus, and Pseudomonas aeruginosa". *Journal of King Saud University – Science.* **34**. 10.1016/j.jksus.2021.101862.

[52] G. Applerot, J. Lellouche, A. Lipovsky, Y. Nitzan, R. Lubart, A. Gedanken, and E. Banin. (2012). "Understanding the antibacterial mechanism of CuO nanoparticles: Revealing the route of induced oxidative stress". *Small.* **8** (21): 3326-3337. 10.1002/smll.201200772.

[53] S. Panda, T. K. Rout, A. D. Prusty, P. M. Ajayan, and S. Nayak. (2018). "Electron transfer directed antibacterial properties of graphene oxide on metals". *Advanced Materials.* **30** (24). 10.1002/adma.201702149.

[54] E. Casals, M. F. Gusta, N. Bastus, J. Rello, and V. Puentes. (2025). "Silver nanoparticles and antibiotics: A promising synergistic approach to multidrug-resistant infections". *Microorganisms.* **13**. 10.3390/microorganisms13040952.

[55] A. M. Martorana, S. Molta, D. Di Silvestre, F. Falchi, G. Deho, and et al. (2014). "Dissecting Escherichia coli outer membrane biogenesis using differential proteomics". *PLoS One.* **9** (6). 10.1371/journal.pone.0100941.

[56] M. Toyofuku, G. Carcamo-Oyarce, T. Yamamoto, F. Einstein, M. Kurosawa, and et al. (2017). "Prophage-triggered membrane vesicle formation through peptidoglycan damage in Bacillus subtilis". *Nature Communications.* **8**. 10.1038/s41467-017-00492-w.